MINERALOGICAL MAGAZINE

VOLUME 61 NUMBER 408 OCTOBER 1997

An EXAFS study of the local structural environments of Fe, Co, Zn and Mg in natural and synthetic staurolites

C. M. B. HENDERSON AND J. M. CHARNOCK

Department of Earth Sciences, University of Manchester, Manchester M13 9PL and Daresbury Laboratory, CLRC, Warrington WA4 4AD, UK

G. CRESSEY

Department of Mineralogy, Natural History Museum, London SW7 5BD, UK

AND

D. T. GRIFFEN

Department of Geology, Brigham Young University, Provo, Utah 84602, USA

Abstract

X-ray absorption spectroscopy (XAS) has been used to study the local structures of Fe, Co, Zn, and Mg in synthetic and natural staurolites. Results for the near-edge features (XANES) and refined EXAFS were used to deduce the crystallographic site(s) occupied for each element. The least squares refined, mean first shell metal-O bond lengths, coordination numbers, and Debye-Waller factors are in the ranges: Fe 1.97–1.99 Å, 3.5–4.1, 0.013–0.023 Å^2; Co 1.97–1.98 Å, 3.5–3.9, 0.009–0.014 Å^2; Zn 1.95–1.96 Å, 3.7–3.8, 0.008–0.009 Å^2; and Mn 1.99 Å, 3.8, 0.012 Å^2. No significant differences were found which depended on element concentration or whether the sampes are synthetic or natural. The refined bond length for Mg in end-member Mg-staurolite is 2.00 Å but EXAFS data did not allow refinement to give reliable coordination number and Debye-Waller factor estimates. The EXAFS data, together with staurolite and model compound XANES features, suggest that > about 90% of Fe, Co, Zn and Mn are concentrated in the tetrahedral T2 site, while in Mg-staurolite > about 75% of the total Mg is in T2 with the remainder in octahedral sites. In natural staurolite from Pizzo Forno (PF2), a greater proportion of Mg appears to be in octahedral coordination.

KEYWORDS: EXAFS, staurolite, XANES, local structural environment.

Introduction

ALTHOUGH natural staurolites show only limited variation in the concentration levels of the major cations Fe, Al and Si, the structural relations are complex in that: (i) the structure consists of seven octahedral and two tetrahedral cation sites, (ii) Fe and Al are distributed over several sites, and (iii) some of these sites are only partially occupied (Smith, 1968). Hawthorne *et al.* (1993*a*) have recently revised the original site nomenclature as follows: four-coordinate sites (T1, T2), octahedral sites (M1A, M1B, M2,

Mineralogical Magazine, October 1997, Vol. 61, pp. 613–625

M3A, M3B, M4A, M4B). In addition to Fe, Al and Si, staurolite contains essential H in variable amounts; minor contents of Ti, Mn and Li are ubiquitous, while Mg, Zn, Co, and Cr are occasionally enriched to percent concentration levels (see e.g. Ward, 1984; Dutrow *et al.*, 1986; Bringhurst and Griffen, 1986; Holdaway *et al.*, 1986*a*; Enami and Zang, 1988; Alexander, 1989; Dutrow, 1991; Hawthorne *et al.*, 1993*a*; Soto and Azañón, 1993, 1994). Such factors have combined to lead to uncertainties in cation site assignments and problems in the adoption of reliable stoichiometric formulae. More detailed structural and stoichiometric information is required to help in obtaining unambiguous thermodynamic properties so that staurolite-bearing assemblages can be used in modelling metamorphic *P-T* conditions (Holdaway *et al.*, 1986*b*, 1991, 1993, 1995).

Several different types of experimental studies have recently improved structural models for staurolite. Hawthorne *et al.* (1993*a,b,c*) used single crystal X-ray diffraction methods to refine the structures of 42 natural samples from 17 different rocks and allocated cations to different structural sites based on electron density distributions, bond valence information, and bond lengths. Hawthorne *et al.* (1993*a*) deduced that total Fe* (Fe^{2+} + Fe^{3+} + Mn + Ti) was, on average, mainly in $^{[4]}$T2 (87%) with the remainder distributed over the octahedral sites in the proportions M4 5.1%, M2 4.5%, M1 2.6%, and M3 0.6%. They also suggested that total Mg was distributed over $^{[4]}$T2 55.8%, and the octahedral sites M1 25.6%, M3 11.6%, M2 7.0%. Dyar *et al.* (1991) studied 23 natural and 12 synthetic staurolites by ^{57}Fe Mössbauer spectroscopy and established that, on average, the total Fe content consisted of 82% Fe^{2+} in $^{[4]}$T2, 5% Fe^{3+} in $^{[4]}$T1 (8% in synthetic samples), 11% Fe^{2+} in octahedral M3 or M4 sites, and a possible charge transfer contribution in some samples. Ståhl *et al.* (1988) determined the structural sites occupied by H using single crystal neutron diffraction for a natural staurolite from Pizzo Forno, Switzerland, and Henderson *et al.* (1993) used the same sample for an element specific, X-ray absorption spectroscopy (XAS) study and established that Fe, Mn, Zn were mainly in T2 with Ti occupying M2. Based on these studies, Holdaway *et al.* (1995) recently defined the general staurolite formula as:

$$H_{2-8}\,{}^{T2}(Fe^{2+}, Mg,Zn,Li,Mn,Al,Fe^{3+},\square)_4\;{}^{M1}(Al,Mg,Fe^{2+})_8\;{}^{M2}(Al,Mg,Fe^{2+},Ti)_8\;{}^{M3}(Al,Mg,Fe^{2+},\square)_4\;{}^{M4}(\square,Fe^{2+},Zn,Li)_4\;{}^{T1}(Si,Al)_8O_{48}$$

Studies of synthetic solid solution series have also provided valuable information on the crystal chemistry of staurolite. Richardson (1967) found that synthetic Fe-Mg staurolites had compositions with 7.5 rather than 8 atoms of Si per formula unit (p.f.u.) in T1. End-member Mg-staurolite synthesized by Schreyer and Seifert (1969) also appears to be Si-deficient and those prepared by Fockenberg (1995) are Si- and Mg-deficient. Griffen (1981) found that Fe-Zn staurolites, and Phillips and Griffen (1986) found that Fe-Co staurolites, both with 7.5Si atoms p.f.u., formed complete solid solution series, with unit cell parameters showing essentially linear relationships with composition. It was suggested that Zn and Co substitute for Fe, not necessarily restricted to substitution on the T2 site.

The element-specific X-ray absorption technique is useful for studying the local structural environments of cations in minerals such as staurolite (Henderson *et al.*, 1993), particularly for element pairs such as Fe-Co and Mg-Al which cannot be distinguished by X-ray diffraction techniques because of their similar scattering properties. However, interpretation of spectra where a given element is distributed over several sites is complicated as the technique provides information on the average environment of the target element. Nevertheless, it is possible to deduce whether or not the element is mainly concentrated in a particular site. XAS spectra consist of several regions (see the review of Brown *et al.*, 1988). Pre-edge, edge and near-edge structure (X-ray absorption near-edge structure, XANES) provide information on valency, coordination number, and site symmetry. Pre-edge and edge features are generally associated with electron transitions to localized states (e.g. the pre-edge in the first series transition elements is due to low-probability, 1s-3d transitions), whereas XANES features result from multiple scattering effects yielding qualitative three-dimensional information. In contrast, data reduction of the Extended X-ray Absorption Fine Structure (EXAFS) gives one-dimensional, radial, short-range (i.e. to about 6 Å) structural information in the form of average bond lengths, coordination numbers, and Debye-Waller factors (disorder parameters). For the first series transition elements, K-edge pre-edge and edge features are particularly rich in structural information (e.g. Waychunas *et al.*, 1983; Waychunas, 1987; Henderson *et al.*, 1993, 1995).

In this paper we show how the results of an XAS study of Fe, Zn and Co K-edges provide further information on the structural environments of these elements in the synthetic Fe-Zn and Fe-Co staurolites mentioned above. We also present Fe and Co data for the natural Co-rich staurolite, lusakite (Skerl and Bannister, 1934) and a cobaltoan staurolite (Cêch *et al.*, 1981; Bringhurst and Griffen, 1986). The development of soft-XAS at the Daresbury SRS, using beryl monochromators, has allowed the first element specific study of Mg environments in a synthetic Mg-staurolite end-member (nominally

10.3 wt.% MgO) and in a natural sample from Pizzo Forno, Switzerland, which contains 2.1 wt.% MgO and the results are also given here.

Experimental trechniques

Synthetic samples for the Fe-Co and Fe-Zn staurolite series are those described in Griffen (1981) and Phillips and Griffen(1986). They were synthesized at 30kbar and 750°C from starting compositions of stoichiometry 4.0 *M*O : 9.0 Al_2O_3 : 7.5 SiO_2, where *M* = Fe, Zn, Co. In addition to the Fe-, Co-, and Zn end-members, intermediate solid solutions of composition $Fe_{0.8}Co_{0.2}$, $Fe_{0.6}Co_{0.4}$, $Fe_{0.4}Co_{0.6}$, $Fe_{0.2}Co_{0.8}$ and $Fe_{0.75}Zn_{0.25}$, $Fe_{0.5}Zn_{0.5}$, $Fe_{0.25}Zn_{0.75}$ were studied. The Mg end-member staurolite was synthesized at Bochum at 20 kbar and 800°C for 3days from a gel of composition 4MgO : $9Al_2O_3$: $8SiO_2$. The Co-rich natural staurolite (lusakite; BM1934,819) studied is that of Skerl and Bannister (1934) which is intimately intergrown with magnetite and quartz so that the sample studied contains impurities of these phases. New microprobe analyses of lusakite BM1934,819 shows that FeO is zoned from 7.5 to 9.9% (mean 8.7%) and CoO from 6.7 to 9.4% (mean 7.6%) with about 0.6% NiO. The natural cobaltoan staurolite studied here is that of Cêch *et al.* (1981) with 9.15 wt.% FeO, 2.52 wt.% CoO. The Pizzo Forno sample studied is PF2 of Holdaway *et al.* (1986) which contains 13.18%FeO, 0.18% MnO, 0.23% ZnO and 2.14% MgO.

Extended X-ray absorption fine structure (EXAFS) spectroscopy experiments were performed at the Daresbury Synchrotron Radiation Source (SRS), operating in multibunch mode at an energy of 2 GeV with an average current of 150 mA. Samples were finely ground under acetone and mounted on aluminium sample holders with Sellotape windows. Fe, Co and Zn *K*-edge EXAFS spectra were collected, at room temperature in transmission mode with ion-chamber detectors, on station 7.1 using a Si (111) double crystal monochromator detuned to 50% rejection of the incident beam in order to remove harmonic contamination. The less concentrated samples were scanned 2 to 4 times and the spectra added together. Zn edges were also collected at liquid nitrogen temperatures in an attempt to establish whether local disorder (Debye-Waller factors) was mainly static rather than thermal in origin. Mg *K*-edge spectra were obtained on station 3.4 using total-electron-yield detection methods, with beryl (100) monochromators. Note that an energy range of only about 250 eV can be obtained before the Al *K*-edge from the beryl monochromators is encountered. Samples were ground and mixed with graphite to prevent charging and mounted on stainless steel sample holders. Because of the low Mg concentration in natural staurolite PF2, the signal:noise ratio was too poor to allow the EXAFS to be refined; thus only XANES spectra could be obtained for this sample.

The raw data were summed in the Daresbury program EXCALIB and background subtracted using EXBACK. The isolated k^3-weighted EXAFS data were analysed using EXCURV92 (Binsted *et al.*, 1991), employing the single scattering spherical wave theory (Lee and Pendry, 1975; Gurman *et al.*, 1984). Phaseshifts were derived from *ab initio* calculations using Hedin-Lundqvist potentials and von Bart ground states (Hedin and Lundqvist, 1969). No Fourier filtering was used. For each spectrum a theoretical fit was obtained by adding shells of backscattering atoms around the central absorber atom and iterating the the Fermi energy correction (E_f), the absorber-scatterer distances (R) and the Debye-Waller type factors ($2\sigma^2$) for all shells, and the coordination number (N) for the first shell only, to get the best agreement with the experimental data. The Debye-Waller factors include contributions from the thermal motion of the absorber-scatterer pairs and also a static contribution from any variation in R between the scatterers in one shell. For modelling the spectra, the number and type of atoms in each shell of back-scatterers was based on those associated with the cation sites defined in Smith (1968) but O atoms beyond 4.6 Å were not included as scattering from these makes an insignificant contribution to the EXAFS. Initially only the first shell was included in the simulation and the outer shells were added sequentially. Statistical tests (Joyner *et al.*, 1987) were used to determine whether addition of a shell made a significant improvement to the fit, and only those significant at the 1% level were accepted. Relative errors in the first-shell bond distance are ± 0.01 Å with probable absolute errors of ± 0.02 Å; outer shell distance errors are somewhat larger. Errors for estimated coordination numbers (first shell only) and Debye-Waller factors are about $\pm 20\%$.

The possible presence of anharmonicity (and anisotropy) in the first shell of oxygens, and thus the possibility that Gaussian fits to the data give anomalously short bond lengths and low coordination numbers, was assessed using the most recent version of EXCURV92 which utilises the method of cumulant expansion. In this method, additive phase-shift ($B = 4/3C_3k^3$; where C_3 is the third cumulant and k the photoelectron wave vector) and multiplicative amplitude ($C = 2/3C_4k^4$; C_4 is the fourth cumulant) terms take account of the effects of anharmonicity on the refined bond-lengths and coordination numbers, respectively (see, for example, Brown *et al.*, 1995).

The Fe, Mn, and Zn K-edge data for Pizzo Forno staurolite PF2 (Henderson *et al.*, 1993) were re-

refined using EXCURV92 and Hedin-Lundqvist-potential-based phase shifts to allow direct comparison with the data reported here.

Results and structural assignments

Fe, Co and Zn

The pre-edge and expanded XANES regions for Fe and Co *K*-edges in the Fe-Co-staurolite solid solution series and in the natural lusakite and a natural cobaltoan staurolite are shown in Fig. 1, and for Fe and Zn in the Fe-Zn staurolite series and natural staurolite PF2 in Fig. 2. Note that clear pre-edge peaks are present for Fe and Co edges but not for Zn. Zinc, of course, contains no holes in the 3d electron shell so that the bound state 1s-3d transition is not possible, even for non-centrosymmetric tetrahedral coordination.

The features shown in these spectra for a given target element are essentially identical. The pre-edge peak heights (Table 1) for Fe in both staurolite series are the same within error (0.075–0.080 relative to the edge step height) and are not significantly different from the Fe pre-edge intensity reported for Fe in natural staurolite PF2 (0.075; Henderson *et al.*, 1993). The fact that the pre-edge peak in the synthetic samples is not significantly larger than in natural staurolite suggests that the Fe^{3+} contents are of the same order. Note that Dyar *et al.* (1991) found that Fe^{3+} averaged about 5% of total Fe in natural samples and 8% in synthetic staurolites. The Co pre-edge peak is constant at 0.070 (relative to the edge step height) in the synthetic samples and in the natural Co-rich staurolites studied. The pre-edge peak height for Mn in PF2 staurolite is 0.10 (Henderson *et al.*, 1993). The decreasing pre-edge heights in the order Mn-Fe-Co-Zn is inversely related to the number of 3d-holes (Mn^{2+} 5, Fe^{2+} 4, Co^{2+} 3, Zn^{2+} 0), reflecting that a larger number of holes leads to a higher probability for the 1s-3d electron transition.

The positions of the XANES features are closely similar for the Fe in all the samples except for the lusakite which contained impurity magnetite (Figs 1 and 2). The inter-sample relative intensities for the staurolite Fe XANES peaks are very similar except that the peak at about 7117 eV shows subtle differences, e.g. it is less clear in the synthetic Fe end-member and better developed in the natural cobaltoan staurolite and in the Pizzo Forno sample (PF2). Co XANES peaks in all the samples are essentially identical, as are those for Zn. Thus, it seems that the relatively long-range structures probed by the multiply-scattered, low kinetic energy XANES photoelectrons are essentially identical irrespective of the concentration of a given element. In addition,

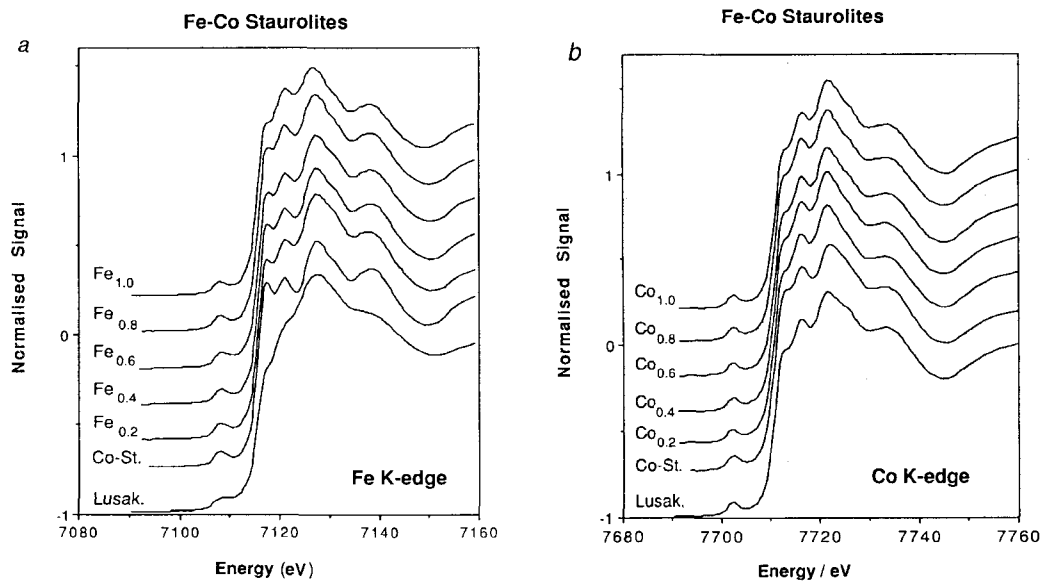

FIG. 1. XANES spectra for synthetic Fe-Co staurolites (e.g. Fe_xCo_{1-x}), natural cobaltoan staurolite (Co-St.) and natural lusakite (Lusak.): (*a*) Fe, (*b*) Co. The spectra are closely similar except that Fe in lusakite shows differences which reflect the presence of impurity magnetite. The Co spectrum for lusakite is identical to those for the other staurolites. Pre-edges for Fe and Co have similar intensities.

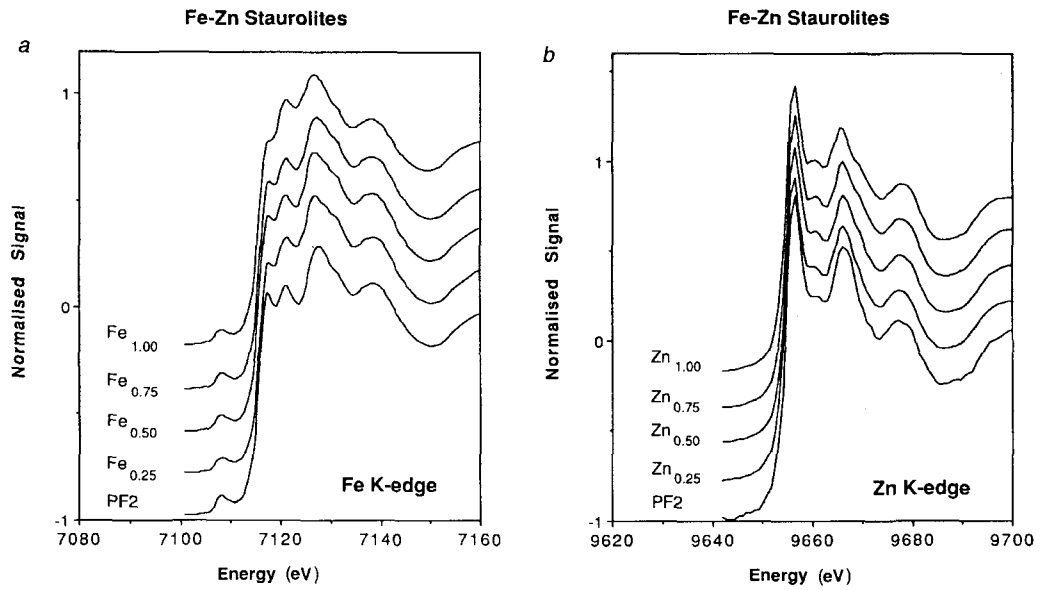

FIG. 2. XANES spectra for synthetic Fe-Zn staurolites and natural Pizzo Forno staurolite (PF2): (*a*) Fe, (*b*) Zn. The spectra for each element are closely similar and the data for Fe are similar to those for Fe in the Fe-Co staurolites in Fig. 1*a*. No pre-edges are present in the Zn spectra.

the positions of the main XANES peaks, relative to the edge energies (E_0), for each of Fe, Co, and Zn (also for Mn in PF2; Henderson *et al.*, 1993) are the same within error (± 0.5 eV) although the relative intensities show some differences (see later, Fig. 8). Overall, the pre-edge and near-edge features indicate that Fe, Co and Zn (also Mn) each occupy the same types of structural environment in all of the samples studied irrespective of whether they are synthetic or natural staurolites.

The experimental EXAFS spectra and Fourier transforms for synthetic end-member Fe-, Co- and Zn- staurolites are shown in Fig. 3; for a given target element, data for the solid solutions and natural samples are essentially identical to those for the end-members except that the signal-to-noise ratio in the more dilute samples is clearly worse than in the more concentrated samples, leading to shorter k ranges available for fitting structural models. The nature of the fine structure features associated with the EXAFS peaks are very similar for all target elements in all staurolites, irrespective of element concentration and whether they are synthetic or natural; in particular, the first EXAFS peak at about 4–5 $Å^{-1}$ in all the staurolites has a distinctive morphology. Figures 4 and 5 show the the EXAFS spectra for the synthetic solid solution series and in natural Co-rich staurolites and PF2; the close similarities indicate that the short range order EXAFS features are diagnostic for 3d metals occurring in closely similar local environments (i.e. the same atomic sites) in staurolite.

Co. The FT peaks show little change in height and width through the synthetic solid solution series. For all the synthetic samples studied, first shell Co–O bond lengths fall in the range 1.97–1.98 Å, while refined coordination numbers and Debye-Waller factors have values in the ranges 3.6–3.9 and 0.009–0.014, respectively (Table 1); none of these differences are significant at the one sigma level. Natural Co-bearing staurolites have refined first shell data not significantly different from these values. For the synthetic Co end-member, we also used the anharmonicity routine in the latest version of EXCURV92 in an attempt to take account of possible distortion in the first shell of oxygens around the target Co. The refined first shell bond lengths and coordination numbers obtained were virtually identical to those obtained using Gaussian fits, as the values to which C_3 and C_4 are related (B and C, above) are at least an order of magnitude smaller than would be necessary for the bond lengths and coordination numbers to show significant shortening.

The outer shells for the synthetic Co end-member and the least concentrated Co staurolite, and the natural lusakite were fitted using theoretical models

TABLE 1. Refined first shell EXAFS data for Fe, Co, Zn, Mg and Mn in synthetic and natural staurolites

	N	R	D.W.	Pre-edge		N	R	D.W.	Pre-edge
Fe-Co series					**Fe-Zn series**				
Fe^{2+}					**Fe^{2+}**				
$Fe_{1.00}$	3.7	1.99	0.023	0.075	$Fe_{0.75}Zn_{0.25}$	3.9	1.98	0.019	0.075
$Fe_{0.8}Co_{0.2}$	3.7	1.99	0.020	0.08	$Fe_{0.5}Zn_{0.5}$	3.9	1.98	0.018	0.075
$Fe_{0.6}Co_{0.4}$	4.1	1.99	0.022	0.08	$Fe_{0.25}Zn_{0.75}$	3.9	1.99	0.018	0.075
$Fe_{0.4}Co_{0.6}$	3.5	1.98	0.013	0.075					
$Fe_{0.2}Co_{0.8}$	3.7	1.97	0.017	0.075	**Zn^{2+}**				
Lusakite	3.7	1.99	0.022	0.045	$Zn_{1.00}$	3.7	1.96	0.008	
Co-staurolite	3.6	1.97	0.013	0.075	$Zn_{0.75}Fe_{0.25}$	3.7	1.95	0.009	
					$Zn_{0.5}Fe_{0.5}$	3.8	1.95	0.009	
Co^{2+}					$Zn_{0.25}Fe_{0.75}$	3.7	1.96	0.009	
$Co_{1.00}$	3.9	1.97	0.012	0.07					
$Co_{0.8}Fe_{0.2}$	3.7	1.98	0.012	0.07					
$Co_{0.6}Fe_{0.4}$	3.7	1.97	0.011	0.07					
$Co_{0.4}Fe_{0.6}$	3.6	1.98	0.009	0.07					
$Co_{0.2}Fe_{0.8}$	3.9	1.98	0.014	0.07	**Mg-staurolite**				
Lusakite	3.5	1.97	0.009	0.07	Mg	4.0*	2.00	0.002	
Co-staurolite	3.9	1.98	0.013	0.07					
Staur. PF2									
Fe	3.5	1.98	0.017						
Zn	3.8	1.95	0.009						
Mn	3.8	1.99	0.012						

N = Coordination number; R = distance from target atom to shell of scatterers (Å); D.W. = Debye-Waller factor ($2\sigma^2$, $Å^2$);
Pre-edge = Height of pre-edge peak relative to absorption edge step height
* All N values refined except that for Mg in end-member Mg staurolite

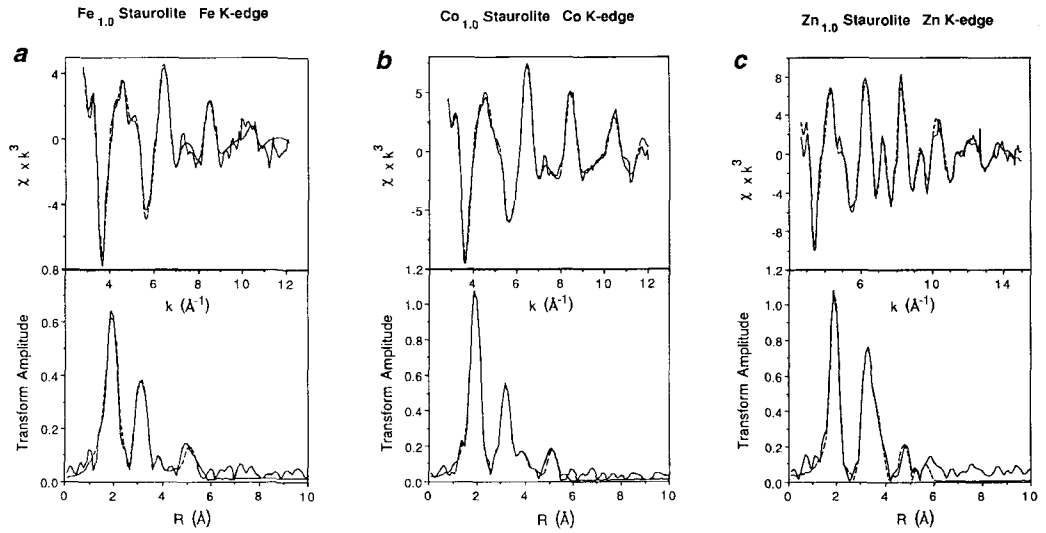

FIG. 3. The k^3-weighted EXAFS ($Å^{-3}$) and Fourier transforms (FT) corrected for phase shifts for synthetic end-member staurolites: (*a*) Fe; (*b*) Co; (*c*) Zn. The solid lines represent experimental spectra and the dashed lines the calculated fits to the parameters for the T2 site given in Table 2.

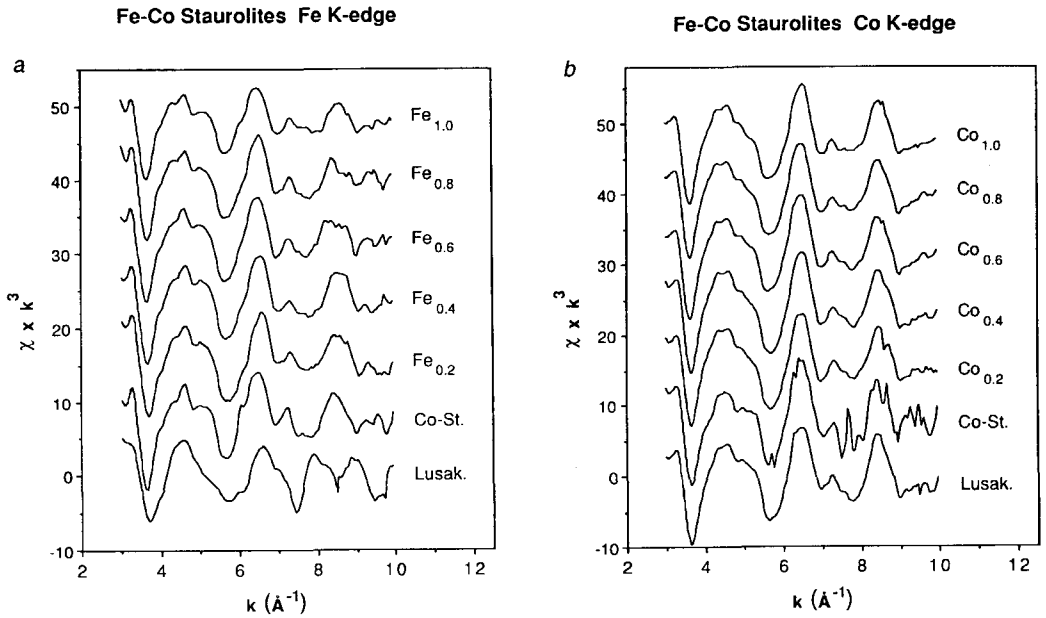

FIG. 4. The k^3-weighted EXAFS ($Å^{-3}$) for the Fe-Co staurolites shown in Fig. 1: (*a*) Fe; (*b*) Co. Spectra are similar for all samples except for Fe in lusakite due to the presence of impurity magnetite.

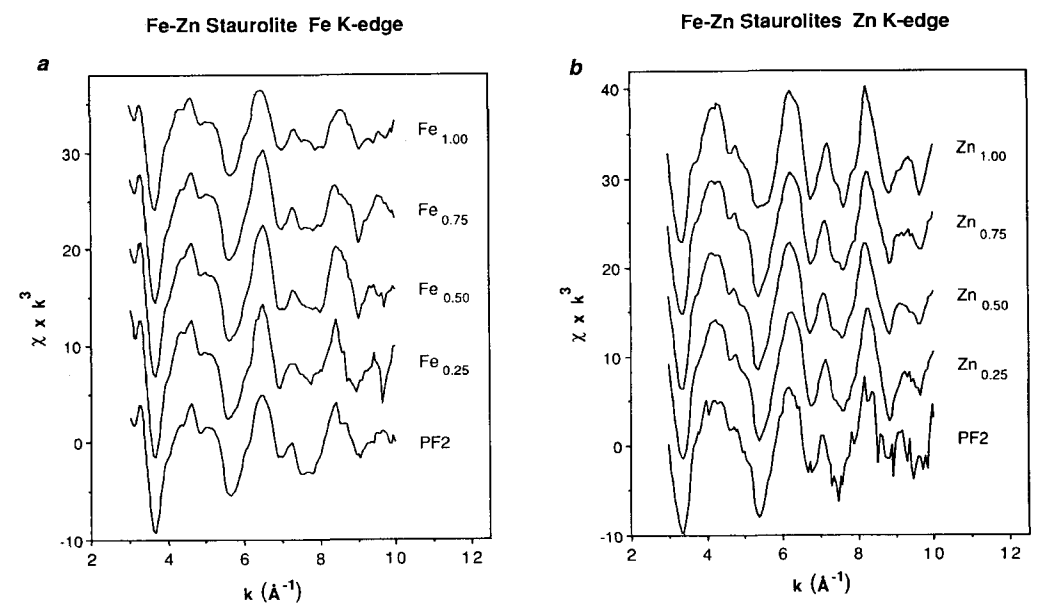

FIG. 5. The k^3-weighted EXAFS ($Å^{-3}$) for the Fe-Zn staurolites shown in Fig. 2: (*a*) Fe; (*b*) Zn. Spectra are similar for each element in all samples.

based on the tetrahedral T2 site, as well as on the octahedral M1, M2, M3, and M4 sites. For each sample, by far the best fit was obtained by using the T2 site to model the Co environment. Only the outer shells characteristic of T2 could fit the detailed structure of the first EXAFS peak at 4–5 $Å^{-1}$ adequately; in particular, the shell of oxygens at about 4.5 Å was required. In addition, for the octahedral site models, the first FT peak could not be fitted by six oxygens; for each sample, the first shell coordination number always refined to less than, but close to, 4 atoms. The FT peak at about 3 Å also showed a particularly poor fit for the M4 environment. Based on these findings, we present the refined data (Table 2 and Fig. 3) for the Co end-member fitted to the T2 shell structure. Because the electron scattering factors for Co and Fe are indistinguishable no attempt was made to fit both element species independently as backscatterers.

The refined bond lengths and Debye-Waller factors for the outer shells give similar values for all samples, irrespective of composition or whether they are synthetic or natural, even though the quality of the fits for the most dilute samples was worse than for more concentrated samples. Thus the data for the Co end-member (Table 2) are representative of the full range of samples. Note that for both the $Co_{1.00}$ and $Co_{0.2}$ synthetic samples, although the Al, Si and O shells in the range 3.0–3.6 Å could not be added separately because of interference, all model shells at >4.5 Å are significant at the 1% confidence level (Joyner *et al.*, 1987). Addition of a metal (Co) shell at 5.8 Å improved the fits to the eye, but was not valid at even the 5% confidence level. Although not explicitly studied, a similar statistical significance for the addition of different shells is expected for all the other samples.

Fe. The peaks in the FT at about 2.0 and 5.0 Å show little variation in both the Fe-Zn and Fe-Co series. However in the Fe-Co staurolites the peak at about 3.2 Å develops a shoulder on the low-R side in the $Fe_{0.8}Co_{0.2}$ sample and a separate peak is resolved at 3.0 Å in the most Fe poor samples; the lower R peak is mainly due to the shell with 2 metal cations. The same splitting is seen in the $Fe_{0.25}Zn_{0.75}$ staurolite sample with peaks at 2.9 and 3.3 Å. The samples showing the better resolution of these peaks are presumably slightly more ordered, i.e. have better crystallinity. The only significant differences in the Fe EXAFS were found for the natural lusakite; the differences can be attributed to a small but significant amount of impurity magnetite as fine-scale inclusions in the mineral separate (Skerl and Bannister, 1934).

TABLE 2. EXAFS radial information for Fe, Co, Zn, and Mg in tetrahedral site T2 for end-member synthetic staurolites

	Shell	N	R	D.W.		Shell	N	R	D.W.
$Fe_{1.00}$	O	3.7#	1.99	0.023	**$Zn_{1.00}$**	O	3.7#	1.95	0.009
	O	6	3.02	0.017		O	6	3.05	0.034
	Fe	2	3.25	0.028		Zn	2	3.16	0.024
	Al	8	3.19	0.095		Al	8	3.39	0.016
	O	6	3.46	0.013		O	6	3.38	0.008
	Al/Si	6	3.61	0.052		Al/Si	6	3.70	0.019
	O	12	4.65	0.078		O	12	4.81	0.018
	Al	10	5.19	0.026		Al	10	5.36	0.025
	Si	4	5.35	0.019		Si	4	5.53	0.005
						Zn	2	5.78	0.008
$Co_{1.00}$	O	3.9#	1.97	0.012	**$Mg_{1.00}$**	O	4.0	2.00	0.002
	O	6	2.93	0.015		O	6	3.01	0.002
	Co	2	3.12	0.013		Mg	2	3.30	0.001
	Al	8	3.05	0.062		Al	8	3.18	0.073
	O	6	3.51	0.025		O	6	3.41	0.001
	Al/Si	6	3.67	0.035		Al/Si	6	3.53	0.011
	O	12	4.55	0.072		O	12	4.73	0.035
	Al	10	5.19	0.019					
	Si	4	5.37	0.016					

Coordination number refined for first shell of oxygens around Fe, Co and Zn only, all other coordination numbers were fixed at the values in the Table.

First shell Fe–O bond lengths for synthetic Fe-Co, Fe-Zn, and natural samples are very similar and in the range 1.97–1.99 Å while refined coordination numbers are within error in the range 3.5–4.1 (Table 1). Debye-Waller factors for the first shell are slightly more variable (0.013–0.023) reflecting some differences between samples in the degree of disorder (Table 1). The relatively high Debye-Waller factor for the lusakite sample presumably is influenced by the presence of impurity magnetite, but the similarly high Debye-Waller factors for the three most Fe-rich synthetic samples suggests that their Fe environments are somewhat more disordered than in the more Fe-dilute synthetic staurolites. Note also that the Debye-Waller factors for Fe are somewhat larger than for Co (Table 1) suggesting that the Fe local environments are more disordered than those for Co.

Henderson *et al.* (1993) stated that the outer shells surrounding Fe in natural staurolite PF2 were much better fitted by the atomic environment associated with the tetrahedral T2 site than with those of any of the octahedral sites. The same relationship has been found in this work for the Fe environments in the representative synthetic $Fe_{1.0}$, $Fe_{0.25}Zn_{0.75}$, and $Fe_{0.2}Co_{0.8}$ samples. The mismatches between the experimental Fe spectra for these synthetic samples and the theoretical spectra for the various octahedral sites are identical to those summarized for Co (above); the same is true for Fe in natural PF2 staurolite. We therefore only present the refined data (Table 2 and Fig. 3) for the synthetic Fe end-member fitted to the T2 shell structure. As found for Co, the fine structure of the first Fe EXAFS peak could only be fitted when the shell of oxygens at about 4.5 Å was included. Because the scattering factors for Co and Fe are indistinguishable no attempt was made to fit element species independently for the Fe-Co series. Fe and Zn have different scattering factors allowing the possibility of detecting clustering of the same element species on adjacent metal ion sites. To investigate this possibility, the shell of cations at about 3.1 Å around the target Fe in the $Fe_{0.25}Zn_{0.75}$ sample was fitted using either two atoms of Fe, or two atoms of Zn, or a stoichiometric mix of Fe and Zn (0.5 atoms Fe, 1.5 atoms Zn). The stoichiometric metal shell gave a better fit than either Fe or Zn independently, pointing to the absence of significant metal ion clustering.

The refined bond lengths and Debye-Waller factors for the outer shells surrounding Fe gave similar values for all samples, irrespective of composition or whether they are synthetic or natural. Thus the data for the Fe end-member (Table 2) are representative of the full range of samples. The statistical qualities of the Fe model fits for the outer shells are similar to those described for the Co spectra.

Zn. The FT peaks at about 2.0 and 3.2 Å show little variation with composition but that at about 5.0 Å appears to become more intense and narrower as the Zn content decreases. The $Zn_{1.00}$, $Zn_{0.5}Fe_{0.5}$, $Zn_{0.25}Fe_{0.75}$ samples were all run at room and liquid nitrogen temperatures but no significant differences in Debye-Waller factors were apparent indicating that, for all shells, the effects of static disorder dominate over those arising from thermal disorder. Despite the smaller signal:noise ratio for the Zn spectrum in PF2 staurolite relative to those in the synthetic samples, the same EXAFS features clearly point to a similar local environment for Zn in all samples.

First shell Zn–O bond lengths in the synthetic series, and in the natural sample PF2, are very similar (1.95–1.96 Å) while refined Debye-Waller factors and coordination numbers are the same within error with values of 0.008–0.009 and 3.7–3.8, respectively (Table 1). Note that the new refinement for the Zn spectrum in PF2 staurolite gives a lower coordination number of 3.8 compared with the value of 5.1 reported by Henderson *et al.* (1993); the new value is more consistent with all the other XAS data reported here. The Debye-Waller factors for the first shell of oxygens around Zn are the smallest of all the elements studied indicating that Zn occupies the least disordered environment of the 3d elements studied.

Henderson *et al.* (1993) found that the outer shells around Zn in natural staurolite PF2 were significantly better fitted by a model for the atomic shell environment centred about the tetrahedral T2 site than with those of any of the octahedral sites. Exactly this relationship has been found in this work for the Zn environments in the synthetic $Zn_{1.0}$ and $Fe_{0.25}Zn_{0.75}$ samples. The mismatches between the experimental Zn spectra for the these synthetic samples (and for PF2) and the theoretical spectra for the various octahedral sites are identical to those summarized for Co and Fe (above). Thus, as found for Co and Fe, the fine structure of the first Zn EXAFS peak could only be fitted when the shell of oxygens at about 4.5 Å around the T2 site was included. Although Fe and Zn have different scattering factors, the shell of metals at about 3.1 Å around the target Zn in the $Zn_{0.25}Fe_{0.75}$ sample showed the same quality of fit for a stoichiometric mix of Fe and Zn to those with entirely Fe or Zn, so the possibility of metal clustering could not be assessed.

The refined bond lengths and Debye-Waller factors for the outer shells surrounding Zn give similar values for all the synthetic samples as well as for PF2. Thus the data for the Zn end-member (Table 2, Fig. 3) are representative of the full range of samples. The statistical qualities of the Zn model

fits for the outer shells are similar to those described for the Fe and Co spectra, however, the quality of the spectra for Zn is such that the FT peak due to a shell of 2 metals at about 5.8 Å is significant at the 1% level in all the synthetic samples.

Mg. XANES spectra for synthetic end-member Mg-staurolite and the natural staurolite PF2 are shown in Fig. 6; the positions of the peaks, in eV, in the synthetic (and natural) sample are 1307 (1308), 1312 (1312), 1317 (1317), and 1329 (1329). Thus the Mg-spectra are essentially identical regarding peak positions although the relative intensities are different, especially those for the first peak. Also shown in Fig. 6 are XANES spectra for model compounds with 4-coordinate Mg in spinel ($MgAl_2O_4$), åkermanite ($Ca_2MgSi_2O_7$), and a synthetic leucite analogue ($Rb_2MgSi_5O_{12}$), and 6-coordinated Mg in MgO and diopside ($CaMgSi_2O_6$). Based on peak positions, the spinel XANES (1307, 1311, 1316, 1329 eV) is closely similar to that for staurolite, and the relative peak intensities for Mg-staurolite and spinel show similarities. Mg XANES peak positions and/or relative intensities in staurolite and spinel are significantly different from those for the other 4-coordinate Mg spectra and for the 6-coordinate model compounds. The implication is that the end-member Mg-staurolite has Mg dominantly in 4-coordination in sites with local geometries similar to those in spinel. Note that Ståhl and Legros (1990) show how the basic staurolite structure can be derived from that of spinel by simple shear and Hollister (1970) remarked on the similarity between the Fe environment in the T2 site and that in hercynite ($FeAl_2O_4$).

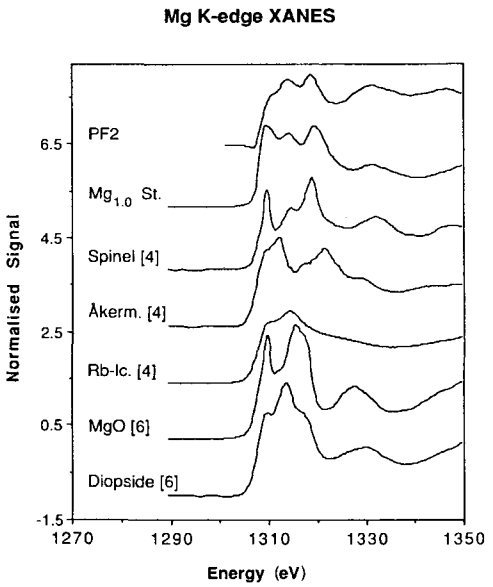

FIG. 6. XANES spectra for Mg in natural staurolite PF2 and synthetic end-member Mg-staurolite, and in synthetic model compounds with: 4-coordinate Mg in spinel ($MgAl_2O_4$), akermanite ($Ca_2MgSi_2O_7$), and Rb-leucite ($Rb_2MgSi_5O_{12}$); and 6-coordinate Mg in MgO, and diopside ($CaMgSi_2O_6$). Note that Mg XANES in end-member staurolite and spinel are similar.

The different relative intensities for the Mg-XANES peaks in natural staurolite PF2 imply that the average local Mg environment in this lower concentration sample (2.3 wt.%) is somewhat different from that in the end-member. Hawthorne *et al.* (1993*a*) convincingly show that total Mg in Pizzo Forno staurolite is about equally divided between T2 (55.8%) and octahedral sites (M1 25.6, M2 7.0, and M3 11.6%). By contrast, they showed that their most Mg-rich natural staurolite (7.8 wt.%) had 34.5% of the total Mg in octahedral M4 with 58.4% in T2, 4.7% in M1, 1.7% in M2 and 0.7% in M3. We will use the refined EXAFS data to analyse whether a significant amount of Mg in synthetic staurolite could be contained in octahedral sites.

Because of the restricted k-range available for the EXAFS of synthetic Mg-staurolite, the FT peaks are relatively broad. The fine structure associated with the first EXAFS peak at 3.5-4.5 $Å^{-1}$ is similar to that observed for Fe, Co, and Zn, which we have shown can only be reproduced by including the outer shells of scatterers associated with the T2 site consistent with the prediction from the XANES that Mg is mainly in tetrahedral coordination. The similar scattering properties of Mg, Al and Si mean that the FT peaks for their shells in the region 3.0–3.5 Å interfere, and cannot be added separately. Although the addition of the 12-fold oxygen shell at 4.7 Å significantly improves the statistics of the fit, the quality of the data does not really justify its addition to the model. The EXAFS data and theoretical model fits are shown in Fig. 7 and the refined parameters (T2 only) summarized in Table 2; note that the coordination number for the first FT shell is fixed at 4.0 as attempts to refine it gave non-physical (negative) Debye-Waller factors, with N refining to an unrealistically low value of 3.3.

Discussion and conclusions

We have commented earlier that XANES features for Fe, Co, Zn and Mn are in similar positions relative to the edge energy (E_o), although the relative intensities for each element are different. These relationships are clearly displayed in Fig. 8 and show that the four most characteristic features for each element occur at about 3.0, 6.7, 12.5, 24.3 (all ± 0.5) eV, relative to

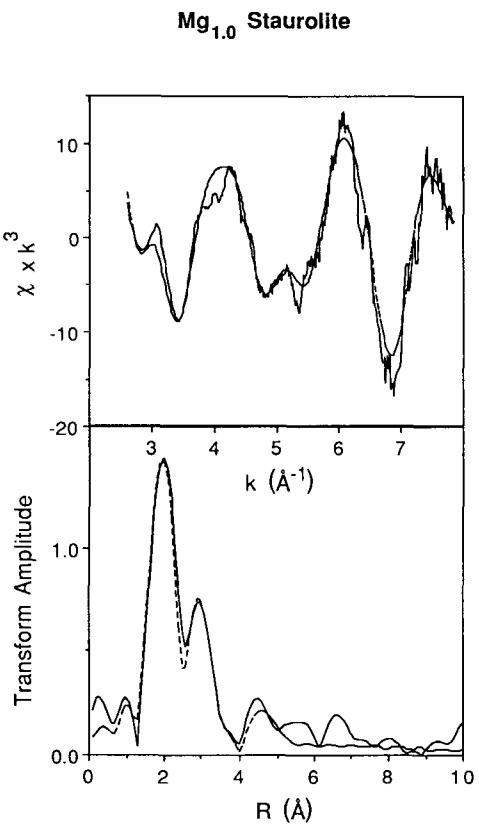

FIG. 7. The k^3-weighted Mg EXAFS ($Å^{-3}$) and Fourier transforms (FT) corrected for phase shifts for synthetic end-member Mg-staurolite. The solid lines represent experimental spectra and the dashed lines calculated fits to the parameters for the T2 site given in Table 2.

E_0. The main differences in relative intensities are shown for the peaks at 3.0 eV which show increasing intensities in the order Fe, Co < Mn < Zn. Such variations reflect fundamentally different electronic structures and/or multiple scattering properties for the different 3d elements in the staurolite structure. If the 3.0eV peak is produced by multiple-scattering resonances, then its intensity may be a measure of the geometrical regularity of the T2 site. The relative intensities observed for this feature may therefore provide a further indication that Fe has the most distorted and Zn a relatively symmetrical site geometry, which is consistent with the EXAFS modelling. For each 3d target element, the close similarities of the longer range XANES features and of the EXAFS spectra point to Fe, Co, Zn, and Mn all being in similar local atomic environments irrespective of concentration. The model fits for shells of atoms surrounding each target element are best fitted by the atomic environment associated with the tetrahedral T2 site.

The XANES features for Mg in synthetic Mg-staurolite and in spinel are very similar (Fig. 6), consistent with Mg being in tetrahedral coordination in staurolite. The positions of the Mg XANES peaks show excellent agreement with those for the 3d elements (Fig. 8). In addition, the fine structure of the first EXAFS peak for Mg in staurolite is similar to that considered to be diagnostic of the T2 site based on the data for Fe, Co and Zn. Thus it appears that the bulk of Mg in this sample is concentrated in the T2 site, but note that the different XANES spectrum for sample PF2 (Fig. 8) points to the Mg in this sample occupying significantly different local environment(s).

We will investigate these structural deductions further using the refined EXAFS data which are summarized in Table 1. The most reliable data from the EXAFS refinements are the first shell M–O bond-lengths and the following discussion is focused on these distances. 'Ideal' bond lengths for tetrahedral (and octahedral) M–O complexes, based on data of Shannon (1976) are: Fe^{2+} 1.98 (2.13); Fe^{3+} 1.84 (2.00); Mn 1.99 (2.18); Co 1.93 (2.10); Zn 1.95 (2.09); and Mg 1.92 (2.07 Å). By contrast, Holdaway *et al.* (1986*b*) have taken account of the partial occupancies of sites, in particular for the T2 site, together with estimated sizes for vacancies, to deduce tetrahedral T2 (and octahedral) M–O bond-lengths, specifically for staurolite, as follows: Fe^{2+} 2.035 (2.18); Fe^{3+} 1.895 (2.045); Mn 2.065 (2.23); Zn 1.975 (2.14); and Mg 1.975 (2.12 Å). Equivalent values for Co would be 1.98 (2.15 Å). From X-ray single crystal structure determinations, Smith (1968) found T2-O bond lengths varying from 1.971 to 2.047 Å (average 2.008 Å) for Pizzo Forno staurolite while Hawthorne *et al.* (1993), for four samples, reported the range 1.971–2.037 Å with a mean value of 2.004 Å. Henderson *et al.* (1993) found a mean first shell, EXAFS distance for Fe–O of 1.99 Å for Pizzo Forno staurolite, with equivalent Mn–O and Zn–O first shell distances of 2.01 and 1.96 Å, respectively. They used such data, together with refined coordination numbers and XANES features, to suggest that >85% of the total Fe and total Mn in Pizzo Forno staurolite (PF2) were located in the tetrahedral T2 site, and that >70% Zn was located in T2.

The first shell bond-lengths determined here for Fe (1.99 Å), Co (1.98 Å), and Zn (1.96 Å) are either very close to or slightly lower than the T2 values adopted by Holdaway *et al.* (1986*b*) consistent with our assignments above. Longer mean bond-lengths would have suggested the presence of a significant amount of these elements in one or more of the octahedral sites. We conclude that these elements

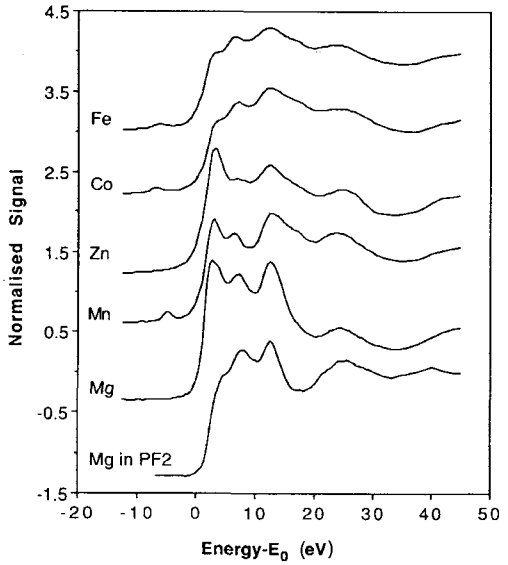

FIG. 8. XANES spectra for synthetic end-member staurolites: Fe, Co, Zn, and Mg; Mn in natural Pizzo Forno staurolite PF2; and Mg in PF2. The energy scale is given relative to the absorption edge position for each element (E_0). Note that for each spectrum, except for Mg in PF2, the peaks for all spectra occur at essentially the same relative energies pointing to the occurrence of the different elements in the same structural site.

(and Mn) are dominantly ordered into the T2 site. Although we cannot be categorical, it seems likely that > about 90% for each element is in T2.

The refined first shell Mg–O bond length of 2.00 Å is significantly longer than those in 4-coordinated model compounds (spinel and akermanite 1.92 Å), which might imply the presence of a major content of octahedral Mg. However, based on the work of Hawthorne *et al.* (1993*a*) and the deductions of Holdaway *et al.* (1986*b*) it seems likely that Mg in the four-coordinate T2 site should have an Mg–O bond length of 1.975–1.982 Å. Equivalent values for Mg–O bond-lengths in staurolite octahedral sites are about 2.06 Å in M1 and M2, 2.10 in M3, and 2.14 Å in M4. Even though EXAFS-derived bond lengths tend to be slightly short for distorted sites, it seems likely that either < about 13% total Mg can be in M4, or < about 17% in M3, or < about 25% in M1 and M2, or some intermediate for distribution over all octahedral sites. Based on both the XANES and refined EXAFS for the synthetic, end-member Mg staurolite we conclude that Mg is dominantly (> about 75%) in tetrahedral T2 sites. The differences in the XANES between the synthetic and natural PF2 staurolite are presumably due to the latter sample containing a smaller proportion of Mg in T2 (cf. 56%; Hawthorne *et al.*, 1993*a*), but our XAS work does not allow even a semi-quantitative estimate.

Finally, although we have found that the bulk of the divalent cations occupy the T2 site, the quatitative estimates are specific to the staurolite samples studied. Thus we have not studied high-H natural samples which would be expected to have a larger proportion of metal cations occupying octahedral sites, especially Fe in M4 (Hawthorne *et al.*, 1993*a*).

Acknowledgements

We thank EPSRC for award of synchrotron beamtime, Dr T. Fockenberg for providing a sample of synthetic end-member Mg-staurolite, Professor F. Cêch for providing the sample of natural cobaltoan staurolite, and Dr F. Mosselmans for obtaining the Fe K-edge spectrum for this sample. We also thank Professor M.J. Holdaway for constructive comments.

References

Alexander, V.D. (1989) Iron distribution in staurolite at room and low temperatures. *Amer. Mineral.*, **74**, 610–19.

Binsted, N., Campbell, J.W., Gurman, S.J. and Stephenson, P.C. (1991) SERC Daresbury Laboratory EXCURV92 program.

Bringhurst, K.N. and Griffen, D.T. (1986) Staurolite-lusakite series. II. Crystal structure and optical properties of a cobaltoan staurolite. *Amer. Mineral.*, **71**, 1466–72.

Brown, G.E., Calas, G., Waychunas, G.A. and Petiau, J. (1988) X-ray absorption spectroscopy: Applications in mineralogy and geochemistry. *Reviews in Mineralogy,* (Min. Soc. Amer.), **18**, 431–512.

Brown, G.E., Jr., Farges, F. and Calas, G. (1995) X-ray scattering and X-ray spectroscopy studies of melts. *Reviews in Mineralogy*, (Min. Soc. Amer.), **32**, 317–410.

Cêch, F., Povondra, P. and Vrana, S. (1981) Cobaltoan staurolite from Zambia. *Bull. Mineral.*, **104**, 526–9.

Dutrow, B. (1991) The effects of Al and vacancies on Li substitution in iron staurolite: A synthesis approach. *Amer. Mineral.*, **76**, 42–8.

Dutrow, B., Holdaway, M.J., and Hinton, R.W. (1986) Lithium in staurolite and its petrologic significance. *Contrib. Mineral. Petrol.*, **94**, 496–506.

Dyar, M.D., Perry, C.L., Rebbert, C.R., Dutrow, B.L., Holdaway, M.J. and Lang, H.M. (1991) Mössbauer spectroscopy of synthetic and naturally occurring staurolite. *Amer. Mineral.*, **76**, 27–41.

Enami, M and Zang, Q. (1988) Magnesian staurolite in

garnet-corundum rocks and eclogite from the Donghai district, Jiangsu province, east China. *Amer. Mineral.*, **73**, 48–56.

Fockenberg, T. (1995) Synthesis and chemical variability of Mg-staurolite in the system MgO-Al_2O_3-SiO_2-H_2O as a function of water pressure. *Eur. J. Mineral.*, **7**, 1373–80.

Griffen, D.T. (1981) Synthetic Fe/Zn staurolites and the ionic radius of $^{IV}Zn^{2+}$. *Amer. Mineral.*, **66**, 932–7.

Gurman, S.J., Binsted, N. and Ross, I. (1984) A rapid, exact curved-wave theory for EXAFS calculations. *J. Phys.*, **C17**, 143–51.

Hawthorne, F.C., Ungaretti, L., Oberti, R., Caucia, F. and Callegari, A. (1993*a*) The crystal chemistry of staurolite. I. Crystal structure and site populations. *Canad. Mineral.*, **31**, 551–82.

Hawthorne, F.C., Ungaretti, L., Oberti, R., Caucia, F. and Callegari, A. (1993*b*) The crystal chemistry of staurolite. II. Order-disorder and the monoclinic → orthorhombic phase transition. *Canad. Mineral.*, **31**, 583–95.

Hawthorne, F.C., Ungaretti, L., Oberti, R., Caucia, F. and Callegari, A. (1993*c*) The crystal chemistry of staurolite. III. Local order and chemical composition. *Canad. Mineral.*, **31**, 597–616.

Hedin, L. and Lundqvist, S. (1969) Effects of electron-electron and electron-phonon interactions on the one-electron state of solids. *Solid State Phys.*, **23**, 1–181.

Henderson, C.M.B., Charnock, J.M., Smith, J.V. and Greaves, G.N. (1993) X-ray absorption spectroscopy of Fe, Mn, Zn, and Ti structural environments in staurolite. *Amer. Mineral.*, **78**, 477–85.

Henderson, C.M.B., Cressey, G. and Redfern, S.A.T. (1995) Geological applications of synchrotron radiation. *Radiat. Phys. Chem.*, **45**, 459–81.

Holdaway, M.J., Dutrow, B.L., Borthwick, J., Shore, P., Harmon, R.S. and Hinton, R.W. (1986*a*) H content of staurolite as determined by H extraction line and ion microprobe. *Amer. Mineral.*, **71**, 1135–41.

Holdaway, M.J., Dutrow, B.L. and Shore, P. (1986*b*) A model for the crystal chemistry of staurolite. *Amer. Mineral.*, **71**, 1142–59.

Holdaway, M.J., Mukhopadhyay, B., Dyar, M.D., Dutrow, B.L., Rumble, D. III and Grambling, J.A. (1991) A new perspective on staurolite crystal chemistry: Use of stoichiometric and chemical end-members for a mole fraction model. *Amer. Mineral.*, **76**, 1910–9.

Holdaway, M.J., Guest, R.F., Mukhopadhyay, B. and Dyar, M.D. (1993) Staurolite end-member molar volumes determined from unit-cell measurements of natural specimens. *Amer. Mineral.*, **78**, 56–67.

Holdaway, M.J., Mukhopadhyay, B. and Dutrow, B.L. (1995) Thermodynamic properties of stoichiometric staurolite $H_2Fe_4Al_{18}Si_8O_{48}$ and $H_6Fe_2Al_{18}Si_8O_{48}$. *Amer. Mineral.*, **80**, 520–33.

Hollister, L.S. (1970) Origin, mechanism, and consequences of compositional sector-zoning in staurolite. *Amer. Mineral.*, **55**, 422–56.

Joyner, R.W., Martin, K.J. and Meehan, P. (1987) Some applications of statistical tests in analysis of EXAFS and SEXAFS data. *J. Phys. C: Solid State Phys.*, **20**, 4005–12.

Lee, P.A. and Pendry, J.B. (1975) Theory of extended X-ray absorption fine structure. *Phys. Revs.*, **B11**, 2795–811.

Phillips, L.V. and Griffen, D.T. (1986) Staurolite-lusakite series. I. Synthetic Fe-Co staurolites. *Amer. Mineral.*, **71**, 1461–5.

Richardson, S.W. (1967) Staurolite. *Carneg. Inst. Washington Yearb.*, **65**, 248–52.

Schreyer, W. and Seifert, F. (1969) High-pressure phases in the system MgO-Al_2O_3-SiO_2-H_2O. *Amer. J. Sci.*, **267A**, 407–43.

Shannon, R.D. (1976) Revised effective ionic radii and systematic studies of interatomic distances in halides and chalcogenides. *Acta Crystallogr.*, **A32**, 751–67.

Skerl, A.C. and Bannister, F.A. (1934) Lusakite, a cobalt-bearing silicate from Northern Rhodesia. *Mineral. Mag.*, **23**, 598–606.

Smith, J.V. (1968) The crystal structure of staurolite. *Amer. Mineral.*, **53**, 1139–55.

Soto, J.I. and Azañón, J.M. (1993) The breakdown of Zn-rich staurolite in a metabasite from the Betic Cordillera (SE Spain). *Mineral. Mag.*, **57**, 530–3.

Soto, J.I. and Azañón, J.M. (1994) Zincian staurolite in metabasites and metapelites from the Betic Cordillera (SE Spain). *Neues Jahrb. Mineral. Abh.*, **168**, 109–26.

Ståhl, K., Kvick, A and Smith, J.V. (1988) A neutron diffraction study of hydrogen positions at 13 K, domain model, and chemical composition of staurolite. *J. Solid State Chem.*, **73**, 362–80.

Ståhl, K. and Legros, P.F. (1990) On the crystal structure of staurolite. The X-ray crystal structure of staurolite from the Pyrenees and Brittany. *Acta Crystallogr.*, **B46**, 292–301.

Ward, C.M. (1984) Magnesium staurolite and green chromian staurolite from Fiordland, New Zealand. *Amer. Mineral.*, **69**, 531–40.

Waychunas, G.A. (1987) Synchrotron radiation XANES spectroscopy of Ti in minerals: Effects of Ti bonding distances, Ti valence, and site geometry on absorption edge structure. *Amer. Mineral.*, **72**, 89–101.

Waychunas, G.A., Apted, M.J. and Brown, G.E. (1983) X-ray K-edge absorption spectra of Fe minerals and model compounds: Near edge structure. *Phys. Chem. Mineral.*, **10**, 1–9.

[*Manuscript received 4 November 1996: revised 6 January 1997*]